Article

TiO$_2$ Nanotubes on Ti Dental Implant. Part 2: EIS Characterization in Hank's Solution

Tullio Monetta *, Annalisa Acquesta, Anna Carangelo and Francesco Bellucci

Department of Chemical Engineering, Materials and Industrial Production, University of Napoli, Piazzale Tecchio 80, 80125 Napoli, Italy; annalisa.acquesta@unina.it (A.A.); anna.carangelo@unina.it (A.C.); bellucci@unina.it (F.B.)

* Correspondence: monetta@unina.it; Tel.: +39-081-7682-403

Abstract: Titania nanotubes are widely studied for their potential applications in several fields. In this paper, the electrochemical characterization of a dental implant, made of commercially pure titanium grade 2, covered by titania nanotubes, when immersed in Hank's solution, is proposed. Few papers were found in the scientific literature regarding this topic, so a brief review is reported, concerning the use of some equivalent circuits to model experimental data. The analysis of results, obtained by using Electrochemical Impedance Spectroscopy, showed that: (i) a good correlation exists between the variation of E_{corr} and the estimated values of the charge transfer resistance for both the bare- and the nanotube-covered samples, (ii) the nanostructured surface seems to possess a more active behaviour, while the effect could be over-estimated due to the real extent of the surface covered by nanotubes, (iii) the analysis of the "n" parameter, used to fit the experimental data, confirms the complex nature of nanostructured layer as well as that the nanotubes are partially filled by compounds containing Ca, P and Mg, when immersed in Hank's solution. The results obtained in this work give a better understanding of the electrochemical behaviour of the nanotubes layer when immersed in Hank's solution and could help to design a surface able to improve the implant osseointegration.

1. Introduction

A large number of scientific works addresses the use of titanium and its alloys in the biomedical field. Titanium, in fact, is considered a suitable biocompatible material since: (i) it is relatively inert and has a good corrosion resistance, (ii) it absorbs proteins from the biological fluids, and (iii) its surface supports growth and cell differentiation of osteoblastic cells that lead to new bone formation [1]. The increasing interest in biomedical applications of titanium can be associated with some specific properties, which can be summarized as in the following [1]:

1. The spontaneous formation in the presence of air and blood of a passivating film of highly biocompatible titanium dioxide, which gives the implant excellent quality for direct contact with the local tissue.
2. The corrosion resistance in air and aggressive media, a property that has a significant influence on the long-term reliability of implants.
3. The ability to influence redox reactions prosthesis–tissue interface that modulates cell and tissue behavior.
4. An improvement, compared with steel and chrome-cobalt alloys, in the images of NMR (Nuclear Magnetic Resonance) and CT (Computed Tomography).
5. 40% lighter than steel, which makes the titanium implants useful tools for microsurgery.

6.　No allergic reactions in patients.

A great effort is still employed to modify the surface of titanium items to obtain an increased corrosion resistance, a superior bioactivity and antibacterial properties [2–5]. As a consequence, a significant number of scientific papers, in recent years, concerns, among others, the rise of oxide layer thickness to increase corrosion resistance in biological fluids [6], the formation of apatite-like layers for bioactivity [7], the use of plasma electrolytic oxidation to obtain surfaces that allow a better osseointegration [8], the study of surface topography to increase the actual surface exposed and appropriate roughness [9,10] and so on. Recently, several research projects addressed the growth of TiO_2 nanotubes on Ti samples, revealing strong fortification of osseointegration, improved samples bioactivity and improved osteoblast adhesion [11–17] as well as the possibility of their use as an anti-inflammatory and/or recovery of antibiotic substances for controlled drug delivery [18–20]. Titania nanotubes could also promote apatite-like deposition; in fact, annealing, by using appropriate temperature, can induce amorphous to anatase phase transformation, allowing some antibacterial activity and improved hydroxyapatite deposition [21].

Despite the broad field of applications and the use of several techniques used for their characterization, less attention has been paid to the use of electrochemical impedance spectroscopy (EIS) to study titanium samples modified by TiO_2 nanotubes growth in simulated body fluid (SBF) like Hank's solution. EIS has been used since the early 1990s to characterize a broad spectrum of materials, like electrical conductive and non-conductive medium, coated and uncoated samples, to determine, i.e., the protective properties of coatings, the effectiveness of surface treatments, the capacity in batteries and so on [22–24]. EIS analysis can be used to model the systems under study applying electrical equivalent circuits that provide an electrical behaviour "equivalent" to that of the material to be characterized. For some applications of EIS, the electrical equivalent circuits are well defined. It is widely accepted, i.e., that the modelling of an unpainted metal, when exposed to an aggressive environment, can be displayed by using a Randles equivalent circuit [25] (named in honour of John Edward Brough Randles) reported in Figure 1, where some linear electrical components are placed in series/parallel to simulate the electrochemical behaviour of the system and to estimate the values of the solution resistance, R_s, the double layer capacitor, C_{dl}, the charge transfer or polarization resistance, R_{ct}, and the reactants/products diffusion impedance, Z_w.
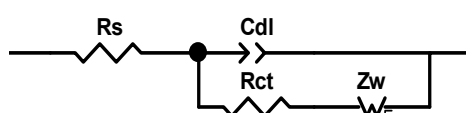

Figure 1. Equivalent circuit employed by Randles to model an unpainted metal [25].

A sketch of the nanotubes layer formed on titanium sheet is reported in the Figure 2. The structure is characterized by the presence of an outer ordinated porous layer (the nanotubes) and an inner compact layer(the barrier layer).
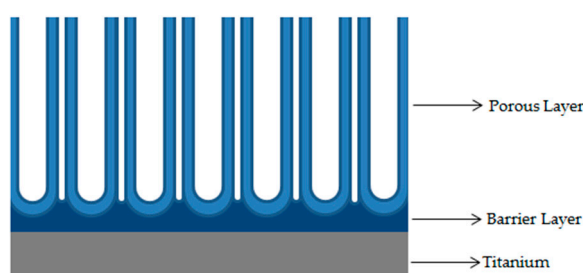

Figure 2. A sketch of the nanotubes layer formed on titanium sheet characterized by the presence of an outer ordinated porous layer and an inner compact layer, known as the barrier layer.

For such kind of complex systems, the analysis of experimental data can be tough to elaborate via EIS, due to the signals overlapping coming from simultaneous phenomena connected with transformation and processes occurring in the sample under testing. For these reasons, researchers can utilize different equivalent circuit models to investigate systems and processes, which can be considered very similar. Part of this paper is devoted to a short literature review on this topic.

The analysis of the literature shows that different models of electrical equivalents circuits have been used when evaluating the properties of titania nanotubes stored in Hank's solution. Typically, each author uses different symbols to indicate the elements of the electrical circuit employed to simulate a real system. If "R" is usually used to indicate an electrical pure resistance, and C, is the symbol used to designate a pure capacitor, several symbols are used to specify a constant phase element (*CPE*). When a capacitor shows a non-ideal behavior, a new type of circuit element can be introduced. It is named "constant phase element" for which acronyms, such as *CPE*, or synonyms QPE or Q, are used. In the following, to avoid confusing the reader, the acronyms used for indicating the circuit elements are those reported by authors in their original papers.

Yu et al. [26] have grown titania nanotubes on flat samples, made in Ti (99.5%), obtaining nanotubes 400 nm in length and 80 nm in diameter. Titanium oxide nanotubes were formed by anodization in a 0.5 wt. %. Hydrofluoric acid (HF) aqueous solution at 20 V for 1 h. Three types of samples were studied: (i) smooth-Ti, (ii) amorphous layer of nanotubes and (iii) anatase layer of nanotubes. The latter were obtained annealing the amorphous sample at 450 °C for 3 h. The electrochemical characterization of samples was conducted in Hank's solution at 37 °C, after 30 min of the open circuit potential measurement, by using the standard three electrodes configuration (titanium specimens as working electrode, platinum and saturated calomel electrode (SCE) as counter electrode and reference electrode, respectively) and recording the data in a frequency range from 100 kHz to 10 mHz.

The equivalent circuit model (reported in Figure 3a) utilized for the analysis of "smooth" sample is composed of a one-time constant circuit, represented as $R_s(R_bQ_b)$, which is usually used for a passive oxide layer. In the model, R_s takes into account the electrolyte resistance, R_b the resistance of the oxide layer, while Q_b is the constant phase elements (*CPE*) of double layer formed on the oxide layer. The model used to study the sample covered by nanotubes (Figure 3b) is composed by two-time constants, represented as $R_s(R_tQ_t)(R_bQ_b)$. The resistance R_s assumes the same meaning as seen before, while R_t and Q_t are, respectively, the resistance and the CPE of the nanotube layer. R_b and Q_b represent the resistance and the *CPE* of the barrier layer. By using the reported models, they obtained an excellent fit quality (the fitted values are shown in Table 1). They found that the corrosion resistance of sample with nanotubes was higher if compared with the sample without nanotubes, due to the higher value of R_b calculated for nanotube covered samples, as evidence of a thicker oxide layer existing in the anodized specimen. Comparing amorphous and annealed samples, the results showed that the annealing had little effect on the corrosion resistance of the inter-barrier layer (R_b) for nanotube layers, but it has a significant effect on the corrosion resistance of the outer tube layer (R_t). This latter effect was attributed to the change of crystallographic structure (from amorphous to anatase) and to the closure of some pores that increases the oxide thickness.
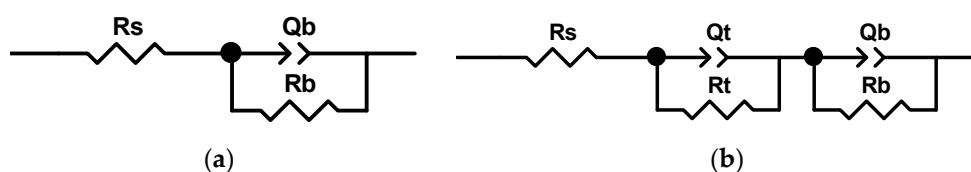

Figure 3. Equivalent circuit model used by [26]: (**a**) for smooth and (**b**) for nanotubes covered samples.

Table 1. Values for the element of the equivalent circuits and chi-squared (χ^2) obtained by Yu [26].

Samples	R_s ($\Omega \cdot cm^2$)	R_t ($\Omega \cdot cm^2$)	Q_t ($S \cdot cm^{-2} \cdot s^{-n}$)	n	R_b ($\Omega \cdot cm^2$)	Q_b ($S \cdot cm^{-2} \cdot s^{-n}$)	n	χ^2
Smooth-Ti	12.3	-	-	-	4.55×10^5	4.93×10^{-5}	0.89	1.00×10^{-3}
Amorphous nanotubes	29.1	326	5.9×10^{-5}	0.63	28.2×10^5	9.4×10^{-5}	0.89	1.00×10^{-4}
Anatase nanotubes	39.7	4696	24.6×10^{-5}	0.79	29.6×10^5	4×10^{-5}	0.97	1.00×10^{-4}

Wen and others [27] utilized Ti CP2 discs (14 mm in diameter, the thickness of 4.0 mm) annealed in an oven at 800 °C. The polished discs (#1500 grit SiC paper with 0.5 mm Al_2O_3 powder) were anodized at 15 V for 2 h in a water solution containing 1.2% HF and 10% H_2SO_4, in order to obtain amorphous titania nanotubes, subsequently annealed at 450 °C for 3 h, obtaining anatase crystallographic structure. The nanotubes diameter was 100 nm, the wall thickness 20 nm and the length of 1.5 μm. The electrochemical characterization of samples was performed by using Hank's solution at 37 °C, for one day and two weeks, in the classical three electrodes configuration as defined before, measuring the data in a frequency range from 10 kHz down to 0.1 Hz. In the paper, various equivalent circuits have been used to take into account the change due to the storage in Hank's solution for two weeks. The equivalent circuit models used for titanium "original," amorphous and anatase nanotubes are reported in Figure 4. The authors employed, considering the anatase nanotubes sample, a model utilized by Aziz-Kerzzo et al. [28] to study experimental data obtained from titanium samples treated with H_2O_2. Aziz-Kerzzo found that the H_2O_2 treatment of Ti surface resulted in the formation of a porous layer on the specimen. By analogy, Wen [27] has used the same model to study the Ti surface covered by nanotubes. The electrical equivalent elements used are: R_s, as the solution resistance, CPE_1 as the constant phase element of the titanium substrate, CPE_{sol} and R_{sol} as the constant phase element and resistance from the inside content of the nanotubes, while CPE_{tube} and W_{tube} are the constant phase element and Warburg diffusion of the nanotubes and W_1 is Warburg diffusion element in series with the solution resistance. Anyway, it is interesting to note that they introduced a diffusivity parameter to take into account diffusion of some ions (Cl^- and Na^+) in the structure.
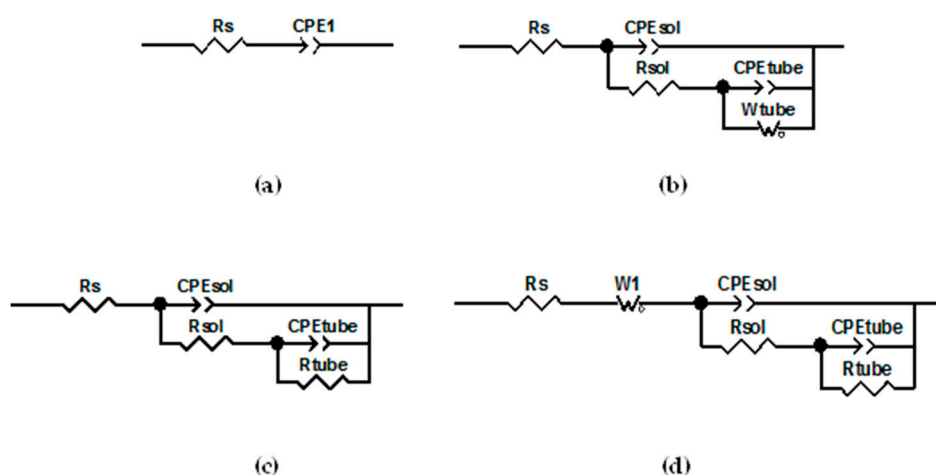
Figure 4. Equivalent circuit model of (**a**) titanium original, (**b**) amorphous nanotubes, (**c**) anatase nanotubes after 1 day of immersion, (**d**) anatase nanotubes after two weeks of immersion [27].

By using the reported models, Wen [27] obtained an excellent fit quality (Table 2). They found instability of amorphous nanotubes regarding a significant variation of impedance modulus at prolonged immersion, while, at the same time, a high stability of anatase nanotubes due to higher impedance values. No indication of the formation of calcium/ phosphorus containing compounds and of apatite-like layers has been reported on amorphous or annealed nanotubes. The change of the

equivalent circuit used to model the data cannot permit a comparison between the values of the parameter found.

Table 2. Values of equivalent circuits obtained by Wen [27].

Samples	Time	R (Ω)	CPE_1 (μF)	W_1 (Ω)	CPE_{sol} (μF)	R_{sol} (Ω)	CPE_{tube} (μF)	W_{tube} (Ω)	R_{tube} (Ω)
Original	1 day	19.19	26.8	-	-	-	-	-	-
	14 days	8.495	18.9	-	-	-	-	-	-
Amorphous	1 day	24.33	-	-	13.5	11072	25.4	30290	-
nanotubes	14 days	29.05	-	-	9	497.7	3.2	2670	-
Anatase	1 day	13.81	-	-	9.4	24.99	9.1	-	833
nanotubes	14 days	10.22	-	15.29	20.6	4065	8.5	-	1763

Al-Mobarak and Al-Swayih [29], following Liu [30], produced titanium nanotubes in three kinds of solutions to obtain nanotubes showing different diameters, varying from 52 to 93 nm, and different length nanotubes, from 250 to 1200 nm. The samples, made of titanium foil (99.5%), were anodized at 20 V for 30 min in the electrolyte made of 1 M Na_2SO_4 and 0.5 wt % NaF (1 solution), or 1 M H_3PO_4 and 0.8 wt % NaF (2 solution), or 0.5 wt % HF (3 solution). The electrochemical measurement was performed in Hank's solution at 37 °C, after 60 min of the open circuit potential measurement. The EIS analysis was carried out in a frequency range from 100 kHz to of 10 mHz, by using the conventional electrochemical cell. The EIS spectra are interpreted by using a model with two-time constants (shown in Figure 5), $R_s(R_1Q_1)(R_2Q_2)$, in which R_s is the solution resistance, R_1 and Q_1 are the resistance and the constant phase element of outer nanotube layer, R_2 and Q_2 are the resistance and constant phase element of the inner barrier layer. The results of modeling are reported in Table 3. The authors assert that: (i) titanium as pristine present two time constants due to the presence of an oxide layer made of a compact passive barrier layer and an outer porous layer; (ii) the diameter dimension affects the electrochemical stability of the nanotubes, in particular, a large diameter leads to decreased corrosion resistance, since nanotubes larger in diameter may include a greater volume of electrolyte, increasing the possibility that corrosion phenomenon can occur.
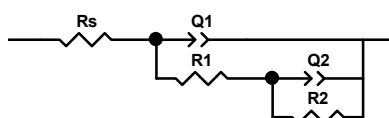

Figure 5. Equivalent circuit model used by [29].

Table 3. Values of equivalent circuits obtained by Al-Mobarak and Al-Swayih [29].

Samples	R_s ($\Omega \cdot cm^2$)	R_1 ($\Omega \cdot cm^2$)	Q_1 ($F \cdot cm^{-2}$)	n_1	R_2 ($\Omega \cdot cm^2$)	Q_b ($F \cdot cm^{-2}$)	n_2
T pristine	42.9	77.9×10^3	0.021×10^{-4}	0.96	909.0×10^3	0.0165×10^{-4}	0.85
T1 (1 sol.)	56.2	14.2×10^3	2.11×10^{-4}	0.95	42.0×10^3	1.76×10^{-4}	0.89
T2 (2 sol.)	43.1	7.95×10^3	3.06×10^{-4}	0.94	36.8×10^3	2.11×10^{-4}	0.91
T3 (3 sol.)	86.1	31.3×10^3	1.91×10^{-4}	0.96	272.0×10^3	0.768×10^{-4}	0.90

Al-Swayih [31] produced titanium nanotubes with diameter from 22 to 75 nm, length from 200 to 830 nm. The samples, made of titanium foil (99.5%), were anodized at 20 V for 30 min in three kinds of electrolyte solutions (inorganic, organic and hybrid one) made of 1 M $(NH_4)_2SO_4$ and 0.5 wt % NH_4F (A), or a mixture of glycerol and water (50:50 vol %) and 0.5 wt % NH_4F (B), or glycerol and 0.5 wt % NH_4F (C). The electrochemical measurement was performed in Hank's solution at 37 °C, after 60 min of the open circuit potential measurement. The EIS analysis was conducted in a frequency range of 10^5 Hz to 10 mHz, using the conventional electrochemical cell. The EIS spectra are interpreted by using a model with two-time constants (reported in Figure 6) $R_1(R_1Q_1)(R_2Q_2)$, in which R_s is the solution resistance, R_1 and Q_1 are the resistance and the constant phase element of outer nanotube layer, and R_2 and Q_2 are the resistance and constant phase element of the inner barrier layer.
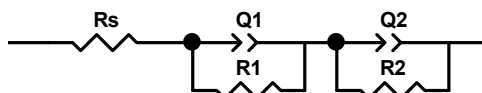
Figure 6. Equivalent circuit used to model EIS spectra of titanium oxide nanotubes sample [31].

Authors highlighted [31] the influence of the electrolyte composition on the nanotubes morphology and, consequently, on their corrosion resistance. In particular, nanotubes anodized in a hybrid solution exhibited a higher corrosion resistance, as indicated by R_2 value (reported in Table 4). In addition, organic components in the solution can facilitate the formation of the well-ordered TiO_2 nanotubes array, while solutions containing only glycerol suppress the formation of nanotubes structures.

Table 4. Values of equivalent circuits obtained by Al-Swayih [31].

Samples	R_s ($\Omega \cdot cm^2$)	R_1 ($\Omega \cdot cm^2$)	Q_1 ($F \cdot cm^{-2}$)	n_1	R_2 ($\Omega \cdot cm^2$)	Q_b ($F \cdot cm^{-2}$)	n_2
A	121.5	2.41×10^3	6.01×10^{-4}	0.91	15.3×10^3	4.4×10^{-4}	0.87
B	96.7	14.8×10^3	2.62×10^{-4}	0.93	131×10^3	1.07×10^{-4}	0.88
C	135.0	6.24×10^3	2.39×10^{-4}	0.92	17.4×10^3	2.61×10^{-4}	0.85

Mohan et al. [32,33] have investigated the electrochemical behaviour of titania nanotubes in Hank's solution, starting from Ti–6Al–7Nb or Ti6Al4V alloys, which although being an interesting application, it is beyond the scope of this paper.

In summary, four papers have used a series/parallel type circuit to describe the nanostructured surface in Hank's solution, while two others have used a dual oxide layer model ($R_s(R_1Q_1)(R_2Q_2)$), as reported in Figure 6. All claim to have obtained very good results from the fitting procedure. The reason why such different equivalent circuits provide an excellent description of nanotubes behavior in Hank's solution is not clear. For example, the diameter and the length of nanotubes do not seem to be relevant variables; in fact, Al-Swayih [31] produced nanotubes varying from 22 to 75 nm in diameter and from 200 to 830 nm in length by using the two-time constants model. Wen [27] found the best fit by using a model containing a Warburg element, when analyzing nanotubes 100 nm in diameter. Al-Mobarak [30], studying nanotubes varying from 52 to 93 nm in diameter and 250 to 1200 nm in length, did not have this need. On the other hand, due to the lack of works available in the field, it is not possible to perform a statistical analysis of the results, in order to find a correlation between the chemical/physical properties of the nanotubes and the electrical equivalent circuit models used. The modeling of the experimental data by using the transmission line model (TLM) could be a useful way to provide a better understanding of the phenomena involved on the Ti surface. Up to today, few papers have been published using this approach as in [34], as we know no one utilizes this method to monitor the apatite-like compounds formation on the Ti surface. Our target is to utilize it and show the results in the next paper of this series.

The experimental results obtained in the present test campaign have been evaluated taking into account both the previous analysis of the literature and the goodness of fitting procedure. Our experimental data have been tested by using several equivalents circuits. Best fitting was obtained by using the dual oxide layer model.

2. Materials and Methods

The samples used in this study are composed by dental implant screws (Deltal Medics, Milano, Italy), 3 mm in diameter and 8 mm in length (Figure 7). They were made in unalloyed titanium, defined as commercially pure grade 2, Ti CP2, (composition is reported in Table 5) as per the ASTM B265–15 Standard Specification for Titanium and Titanium Alloy Strip, Sheet, and Plate [35]. The screws have been pickled in hydrochloric acid solution (10 wt. %) and nitric acid solution (10 wt. %) for 20 min, in order to stabilize the natural oxide layer of the implants. In fact, the machined items could be covered by several types of oxides or showing oxides with different thickness, due to the

thermal stresses to which they are subjected during the processing. The water solution containing HCl and HNO_3 can remove this oxide layer allowing the formation of more stable and uniform coat [36]. The acronyms of samples were: (i) AS to specify the samples pickled and (ii) NT samples with nanotubes.

Table 5. Chemical composition (wt %) of Ti CP2.

Ti	O	N	H	C	Fe
99.7	0.25	0.03	0.015	0.1	0.15

Figure 7. A picture of the dental implant covered by TiO_2 nanotubes [37].

TiO_2 nanotubes were formed by potentiostatic anodizing, at room temperature; in an aqueous solution containing H_3PO_4 (10 wt %) and HF (0.5 wt %), the applied potential was 25 V for durations of 150 min [37].

The electrochemical cell used for anodizing consisted of the titanium screw used an anode and a platinum foil utilized as the cathode. Uniform nanotube distribution on the whole screw was obtained by mounting the sample on a rotating apparatus; the rotation speed was set at 10 rpm. The experimental set-up is represented in Figure 8.
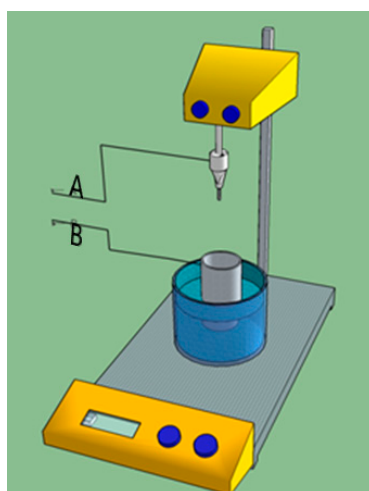

Figure 8. The simple set-up used for nanotubes growth on titanium implant, cables (**A**) and (**B**) were connected to the power supply [37].

A laboratory mixer has been used to hold the screw, a conductive support, connected to the stirrer, permitted the connection between the specimen and the positive pole of the power supply (Gen 600-5.5, TDK Lambda, Milano, Italy). The specimens were rinsed with deionized water and dried in the air after anodizing.

The description of nanotube formation has been reported in [17], their physical and electrochemical characterization is described in [37]. Briefly, the scanning electron microscopy SEM images confirmed that the nanotubes array covered the whole screw and the X-ray Diffraction XRD analysis showed that the screws are covered by an amorphous oxide.

The electrochemical impedance spectroscopy (EIS) tests were conducted by using a three electrodes configuration, including a saturated calomel reference electrode (SCE), a platinum electrode as counter electrode and the titanium sample as working electrode, connected to a potentiostat/galvanostat, 1286 and an electrochemical interface 1287 Solartron (Photo Analytical Srl, Milano, Italy). The area of specimens, exposed to the standard Hank's aqueous solution (Sigma-Aldrich, Milano, Italy, its composition is reported in Table 6), was estimated to be about 3 cm^2. Measurements were carried out at the corrosion potential, E_{corr}, measured vs. SCE, imposing 10 mV of the amplitude of the AC signal, from 20 kHz down to 0.02 Hz, up to an immersion time of 15 days (360 h) at 37 °C. E_{corr} values have been recorded at the beginning of each test. The Zview 2.1b software (Scribner Associates Inc., Southern Pines, NC, USA) was used to model and fit experimental data, and 100 interactions were used to improve the quality of the fit. The routine "Complex", as type of fitting, was used, while "Calc-modulus", as type of data weighting was used. The chi-squared (χ^2) value has been considered to evaluate the goodness of fit, if the value of $\chi^2 \leq 1.0 \times 10^{-3}$ the fitting is considered a good [38].

Table 6. Chemical composition of Hank's solution.

Inorganic Salts Component	g/L
$CaCl_2 \cdot 2H_2O$	0.185
$MgSO_4$	0.09767
KCl	0.4
KH_2PO_4	0.06
$NaHCO_3$	0.35
NaCl	8.0
Na_2HPO_4	0.04788
D–Glucose	1.0
Phenol Red Na	-
$NaHCO_3$	-

3. Results and Discussion

In Figure 9, the Bode and phase angle plot acquired for the sample AS, when immersed in Hank's solution for a duration of 360 h, are displayed. Data highlighted the dynamic nature, and therefore the reactivity, of the spontaneously formed oxide on the implant. In fact, after 24 h of immersion, a shift toward lower phase angle values, at low frequencies, can be observed, while, after 96 h of exposure to test solution, the phase angle increases. This oscillating behavior has been detected until the end of the experimental campaign, as can be observed in the close-up picture reported in Figure 9b. This effect has been associated with the interaction between the TiO_2 oxide surface and the electrolytic solution, containing several anions and cations other than oxygen.
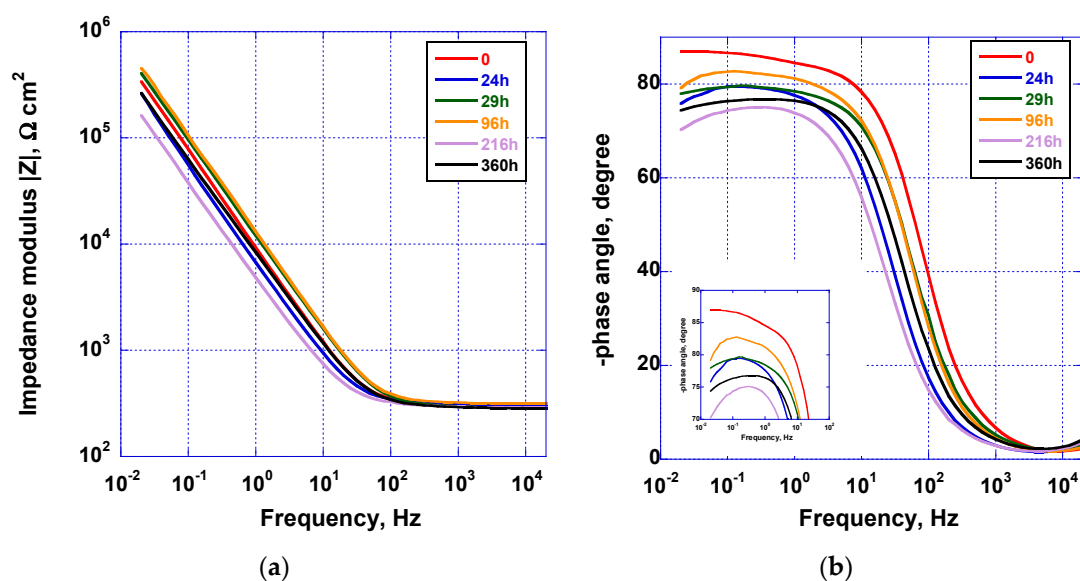
Figure 9. Bode (**a**) and phase angle (**b**) plot acquired for the sample AS when immersed in Hank's solution for a duration of 360 h.

In fact, previous results [37] have demonstrated that the implant surface, at the end of tests, does not show apatite-like deposition layer. Hence, the change in impedance modulus and phase angle can be linked to a continuous remodeling of the surface showing reconstruction and dissolution of oxide.

The analysis of experimental data has been performed by using the equivalent circuit models reported in Figure 10. At the beginning of test campaign (t = 0), the model was constituted by a R_0QPE_0 circuit (Figure 10a), in which R_0 represents the resistance of electrolytic solution and QPE_0 is the constant phase element that takes into account the non-ideal behavior due to the double layer capacitance at oxide/solution interface. For longer exposure time, the experimental data need to be fitted by using the model reported in Figure 10b, in which R_s is the resistance of electrolytic solution, R_{ox} the charge transfer resistance of oxide/solution interface and QPE_{ox} is the constant phase element of double layer at the interface.
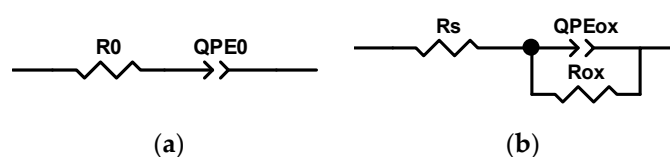

Figure 10. Equivalent circuit used to model EIS data of the AS sample: (**a**) at the beginning of the test (0 h) and (**b**) for a prolonged time of immersion.

The equivalent circuit, reported in Figure 10b, fitted the experimental data obtained starting after 24 h of immersion in the test solution by showing low values of error, while to model the experimental data recorded at the beginning of the test campaign, i.e., at t = 0, the model reported in Figure 10a, has to be employed. In fact, as can be seen from Figure 9b, the sample as the measurement starts has shown, at low frequencies, a capacitive behavior (phase angle value equal to about 87 degrees). The physical implication of this occurrence is that, at t = 0, the charge transfer resistance is very high, suggesting that reaction rate occurring at the interface is very low. When the reaction starts, the equivalent circuit, used to model the data, changes in the circuit reported in Figure 10b.

A significant relationship has been found comparing the corrosion potential, recorded at the beginning of each EIS measurement, and the estimated R_{ox} values obtained fitting the EIS data (reported in Table 7). As can be seen from Figure 11, the R_{ox} value follows the variation of the corrosion potential, showing an increase until 96 h of exposure to the test solution, and then a

decrease followed by a little rise. This occurrence confirms the hypothesis that surface of the untouched screw, when immersed in Hank's solution, is subjected to a reorganization instead of a degradation. A thin porous oxide layer formed when exposed to air covers the untreated implant. When immersed in Hank's solution, which contains a certain amount of salts and oxygen dissolved in it, at pH = 7.4, some chemical reactions are triggered, determining the increase of the oxide layer thickness caused by the presence of oxygen and the slightly basic pH, dealing with a little increase of R_{ox}. In the same time, an increase of E_{corr} occurs, due to the decrease of the extension of the surface occupied by the anodic areas, while cathodic oxide protected areas expand. Then, the system restructures its surface (decreasing R_{ox} and E_{corr}) trying to reach a new equilibrium state.

Table 7. Value of circuit equivalent elements for AS samples.

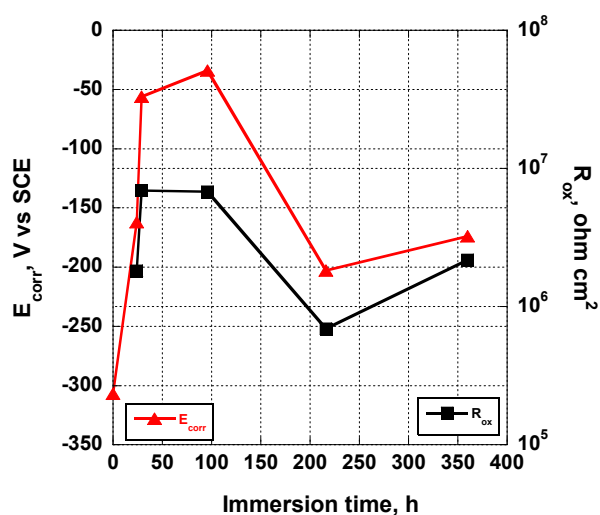| Immersion Time (h)	E_{corr} (mV)	R_0 ($\Omega \cdot cm^2$)	QPE_0 ($F \cdot cm^{-2}$)	n_0	R_s ($\Omega \cdot cm^2$)	QPE_{ox} ($F \cdot cm^{-2}$)	n_{ox}	R_{ox} ($\Omega \cdot cm^2$)	χ^2
0	−307	326.1	1.94×10^{-5}	0.95	-	-	-	-	0.0041
24	−162	-	-	-	310.6	2.76×10^{-5}	0.90	1.81×10^{-6}	0.0046
29	−56	-	-	-	289.7	1.58×10^{-5}	0.90	6.92×10^{-6}	0.0011
96	−34	-	-	-	316.3	1.43×10^{-5}	0.92	6.80×10^{-6}	0.0014
216	−203	-	-	-	292.1	3.99×10^{-5}	0.88	6.90×10^{-6}	0.0063
360	−174	-	-	-	285.7	2.38×10^{-5}	0.88	2.18×10^{-6}	0.0019

Figure 11. Variation of E_{corr} and R_{ox} as a function of time of immersion in Hank's solution displayed by the AS sample.

In Figure 12, the modulus of impedance and phase angle plots acquired for the sample NT, when immersed in Hank's solution for duration of 360 h, are displayed. As can be seen, a two-time constants equivalent circuit (reported in Figure 13) is needed to model the experimental data obtained studying the NT sample.
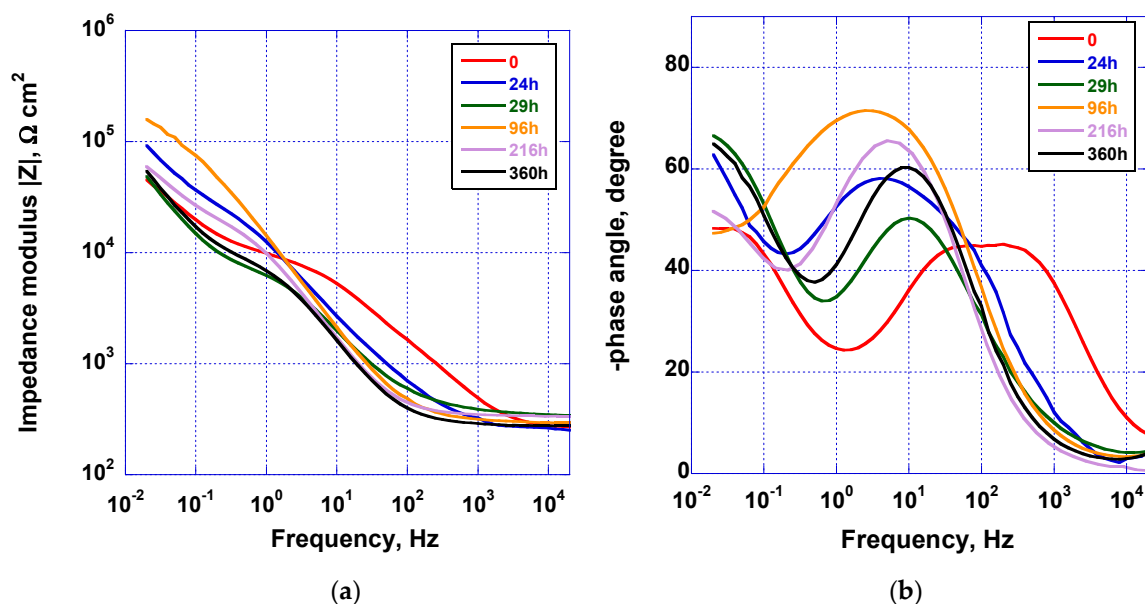
(**a**)　　　　　　　　　　　　　　　　　　　　　　　　　　(**b**)

Figure 12. Bode (**a**) and phase angle (**b**) plot acquired for the sample NT when immersed in Hank's solution for a duration of 360 h.
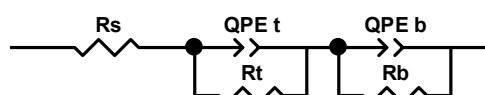

Figure 13. Equivalent circuit used to model EIS data of the NT sample.

The fit's results, reported in Table 8, allow analysing the interaction between the NT sample and Hank's solution. In the same table, the E_{corr} values, measured at the time indicated, are also reported.

Table 8. Values of circuit equivalent elements of NT samples.

Immersion Time (h)	E_{corr} (mV)	R_s ($\Omega \cdot cm^2$)	R_t ($\Omega \cdot cm^2$)	QPE_t ($F \cdot cm^{-2}$)	n_t	R_b ($\Omega \cdot cm^2$)	QPE_b ($F \cdot cm^{-2}$)	n_b	X^2
0	−254	236.8	1.03×10^4	9.87×10^{-6}	0.65	1.40×10^5	1.10×10^{-4}	0.83	0.0031
24	−176	310.1	2.84×10^4	2.13×10^{-5}	0.73	2.17×10^6	8.02×10^{-4}	0.9	0.0040
29	−268	353.3	7.32×10^3	2.52×10^{-5}	0.74	3.32×10^5	1.39×10^{-3}	0.92	0.0019
96	−195	298.9	8.32×10^5	3.67×10^{-5}	0.77	5.47×10^4	2.48×10^{-5}	0.9	0.0014
216	−234	336.4	1.92×10^4	2.14×10^{-5}	0.84	1.88×10^5	1.17×10^{-4}	0.92	0.0004
360	−258	273.4	8.72×10^3	2.51×10^{-5}	0.81	3.15×10^5	1.24×10^{-4}	0.91	0.0009

The complex behavior showed by the NT sample is highlighted by the changes of the values exhibited by the fitting parameters (Figure 14). R_t and R_b values are oscillating for the duration of the test, varying from 7.32×10^3 Ω to 8.32×10^5 Ω cm² and from 5.45×10^4 to 2.17×10^6 Ω cm², respectively, demonstrating high activity of the sample due to the contact with Hank's solution. In our previous paper [37], the formation/dissolution of a protective layer on the nanotubes surface has been assumed and, due to their shape, in the gap between the nanotubes. Shortly after, during the immersion in the test solution, the surface is covered by spots of salt deposited from Hank's solution. Due to the pH slightly acid existing at the bottom of the nanotubes, if compared to the pH of the solution, precipitation/dissolution of chemicals, containing Ca, P, Mg, can occur on the overall nanotube surfaces. These processes lead to a variation of E_{corr} value and the fitting parameters of the equivalent circuit.
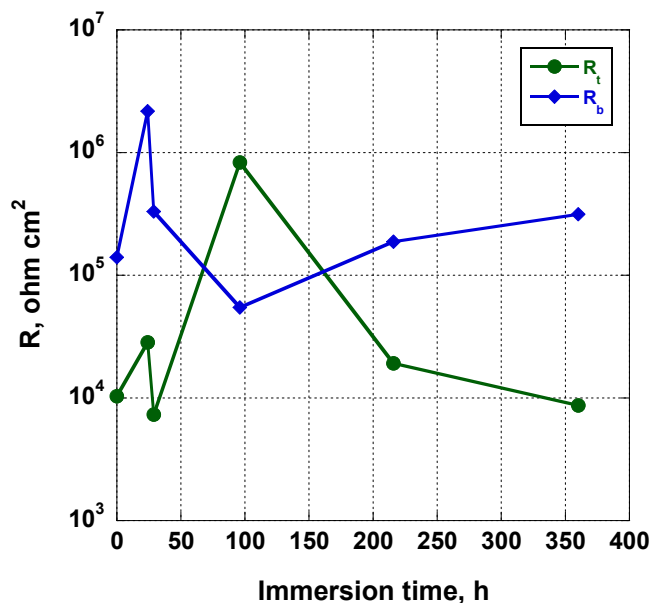
Figure 14. Variation of R_t and R_b as a function of time of immersion in Hank's solution displayed by the NT sample.

The hypothesis is confirmed by the trend of E_{corr} values when compared to R_t (Figure 15). In fact, a good relationship has been found comparing their variation: the R_t estimated value follows the change of the corrosion potential with a good approximation. As seen before, analyzing the case of sample AS, a similar behavior was found comparing values acquired by R_{ox} and E_{corr}. Even if the similarity exists for both the samples AS and NT, the nature of this correspondence is different. In the first case, it can be related to the reorganization of the surface, while, in the former, it can be addressed to surface reorganization and deposition of salts from Hank's solution. In fact, while the R_{ox} variation, for the AS sample, is of about one order of magnitude (varying from $6.90 \times 10^5 \ \Omega$ to $6.80 \times 10^6 \ \Omega \ \text{cm}^2$), the R_t values change of two order of magnitude (from 7.32×10^3 to $8.32 \times 10^5 \ \Omega \ \text{cm}^2$), this effect can be attributed to the deposition of some insulating compounds containing Ca, P and Mg. Nevertheless, comparing the values assumed by R_{ox} and R_t, (without taking into account synergic effect due to the barrier layer on the overall corrosion resistance of the nanostructured sample), it seems that the NT sample showed a more active behavior (see Figure 16). In our opinion (we are collecting more experimental data by using Brunauer–Emmett–Teller analysis to confirm this hypothesis that will be discussed in the third part of this series of papers), the real extent of exposed area of the coated sample is much higher related to the uncoated one. In this way, the estimated values of R_t should be much greater than that obtained by using the geometric area of the sample, as is usually reported in the scientific literature.

The QPE elements, used in the modeling of the experimental data using the equivalents circuits, are utilized to take into account the non-ideal behavior of capacitors to be employed in the simulation. The impedance of a constant-phase element is defined as $Z_{QPE} = 1/(Q(j\omega)^n)$, where $-1 \leq n \leq 1$. The "n" values can be associated to the bulk or surface inhomogeneity of structures under analysis. As reported in Table 7, n_{ox} varied from 0.88 to 0.92, while n_b ranged from 0.83 and 0.92 (Table 8), showing that the oxide formed on the AS sample and the barrier layer oxide of the NT sample possessed a compact structure so that themselves behaved like quasi-ideal capacitors. The n_t values varied between 0.65 and 0.84, highlighting the non-homogenous structure of the nanotubes layer and the effect of the inorganic compounds deposited, which partially filled the pores [37].
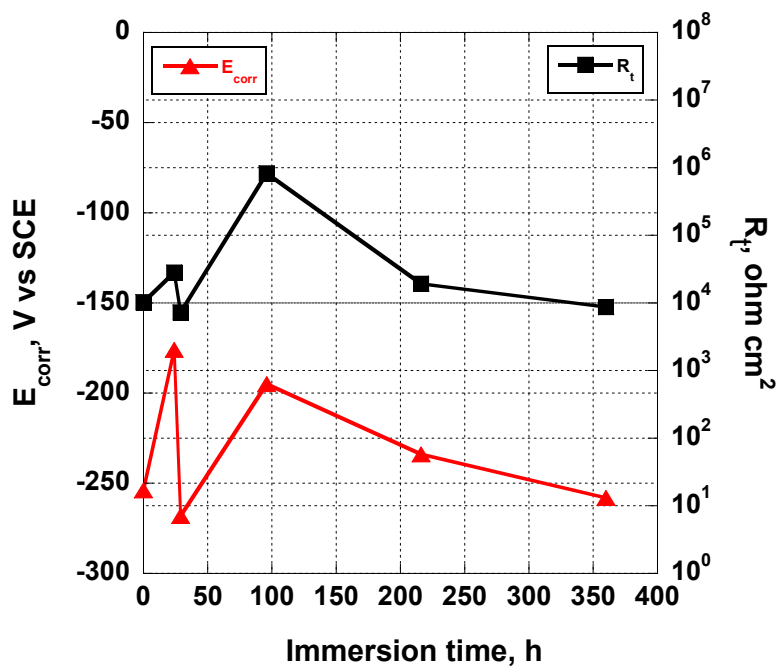
Figure 15. Variation of E_{corr} and R_t as a function of time of immersion in Hank's solution displayed by the NT sample.
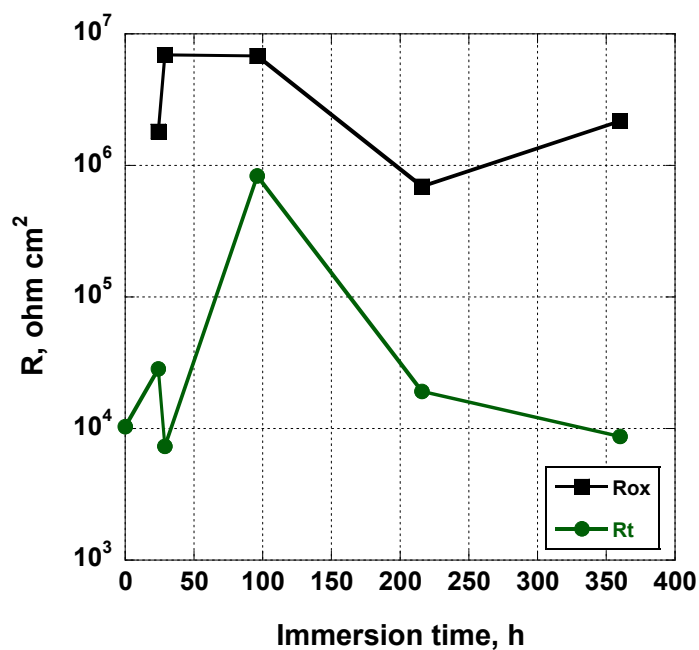

Figure 16. Variation of R_{ox} and R_t as a function of time of immersion in Hank's solution displayed by the NT sample.

4. Conclusions

Results obtained in this study can be summarized as in the following:

1. The analysis of experimental EIS data, by using equivalent circuits models, is a widely used and powerful technique to investigate the variation of electrochemical parameters. In the case of titanium surface covered by nanotubes, different authors have used different equivalent circuits

to model the experimental data acquired. The reason why this can happen is not clear, as few data are available in scientific literature.

2. A good correlation was found between the variation of the measured values of E_{corr} and the estimated values of the charge transfer resistance for both the bare- and the nanotube-covered samples. While the variation assumes a similar trend, the cause of the change is due to different processes.

3. Comparing the fitted charge transfer resistance data, obtained by using the proposed models for bare- and nanotube-covered titanium surfaces, a more active behavior can be addressed for the nanostructured surface. This effect could be over-estimated due to the effective extent of the surface covered by nanotubes.

4. The estimated values of parameter "n" of the constant phase elements confirm the homogeneous structure of both oxide formed on a bare sample and barrier type oxide of samples covered by nanotubes.

5. Estimated values of n_t highlight the non-homogeneity of the nanotube layer and confirm that it is partially filled by compounds containing Ca, P and Mg.

6. The growth of titania nanotubes on the implant surface promote the deposition if compounds contain Ca, P when immersed in the Hank's solution. This effect can help osseointegration of the medical device.

Author Contributions: Annalisa Acquesta wrote the paper and elaborated the data; Anna Carangelo did in-depth bibliographic research; Tullio Monetta conceived the project and made a substantial contribution to the interpretation of the data; and Francesco Bellucci revised the paper critically for important intellectual content.

Conflicts of Interest: The authors declare no conflict of interest.

References

1. Brunette, D.M; Tengvall, P.; Textor, M.; Thomsen, P. *Titanium in Medicine*; Springer: New York, NY, USA, 2001; p. 1019.

2. Monetta, T.; Bellucci, F. Strong and durable antibacterial effect of titanium treated in Rf oxygen plasma: Preliminary results. *Plasma Chem. Plasma Process.* **2014**, *34*, 1247–1256.

3. Monetta, T.; Scala, A.; Malmo, C.; Bellucci, F. Antibacterial activity of cold plasma-treated titanium alloy. *Plasma Med.* **2011**, *1*, 205–214.

4. Nayak, S.; Nanda, K.K.; Rath, P.C.; Bhattacharjee, S.; Chaudhary, Y.S. An investigation on the effect of morphologies on corrosion behaviour of nanostructured hydroxyapatite-titania scaffolds. *J. Bionanosci.* **2010**, *4*, 87–91.

5. Yue, C.; Yang, B. Bioactive titanium surfaces with the effect of inhibiting biofilm formation. *J. Bionic Eng.* **2014**, *11*, 589–599.

6. Lausmaa, J.; Kasemo, B.; Mattsson, H.; Odelius, H. Multi-technique surface charaterization of oxide films on electropolished and anodically oxidized titanium. *Appl. Surf. Sci.* **1990**, *45*, 189–200.

7. Yang, B.; Uchida, M.; Kim, H.M.; Zhang, X.; Kokubo, T. Preparation of bioactive titanium metal via anodic oxidation treatment. *Biomaterials* **2004**, *25*, 1003–1010.

8. Sáenz de Viteri, V.; Bayón, R.; Igartua, A.; Barandika, G.; Moreno, J.E.; Peremarch, C.P.J.; Pérez, M.M. Structure, tribocorrosion and biocide characterization of Ca, P and I containing TiO_2 coatings developed by plasma electrolytic oxidation. *Appl. Surf. Sci.* **2016**, *367*, 1–10.

9. Monetta, T.; Acquesta, A.; Bellucci, F. Evaluation of roughness and electrochemical behavior of titanium in biological environment. *Metall. Ital.* **2014**, *106*, 13–21.

10. Monetta, T.; Marchesano, G.; Bellucci, F.; Lupo, G.; Itro, A. Assessing the roughness of titanium dental implants. *Dent. Cadmos* **2014**, *82*, 498–508.

11. Kim, D.; Ghicov, A.; Albu, S.P.; Schmuki, P. Bamboo-type TiO_2 nanotubes: Improved conversion efficiency in dye-sensitized solar cells. *J. Am. Chem. Soc.* **2008**, *130*, 16454–16455.

12. Roy, P.; Berger, S.; Schmuki, P. TiO_2 nanotubes: Synthesis and applications. *Angew. Chem. Int. Ed.* **2011**, *50*, 2904–2939.

13. Tsuchiya, H.; Macak, J.M.; Müller, L.; Kunze, J.; Müller, F.; Greil, P.; Virtanen, S.; Schmuki, P. Hydroxyapatite growth on anodic TiO_2 nanotubes. *J. Biomed. Mater. Res. Part A* **2006**, *77A*, 534–541.

14. Xiao, P.; Fang, H.; Cao, G.; Zhang, Y.; Zhang, X. Effect of Ti^{n+} defects on electrochemical properties of highly-ordered titania nanotube arrays. *Thin Solid Films* **2010**, *518*, 7152–7155.

15. Yin, L.; Ji, S.; Liu, G.; Xu, G.; Ye, C. Understanding the growth behavior of titania nanotubes. *Electrochem. Commun.* **2011**, *13*, 454–457.

16. Wang, J.; Fan, H.; Zhang, H.; Chen, Q.; Liu, Y.; Ma, W. Anodizing process of titanium and formation mechanism of anodic TiO_2 nanotubes. *Prog. Chem.* **2016**, *28*, 284–295.

17. Monetta, T.; Bellucci, F. Formation of a uniform distribution of TiO_2 nanotubes array on complex geometry samples. *Adv. Sci. Focus* **2013**, *1*, 6–8.

18. De Santo, I.; Sanguigno, L.; Causa, F.; Monetta, T.; Netti, P.A. Exploring doxorubicin localization in eluting TiO_2 nanotube arrays through fluorescence correlation spectroscopy analysis. *Analyst* **2012**, *137*, 5076–5081.

19. Khoshnood, N.; Zamanian, A.; Massoudi, A. Tailoring in vitro drug delivery properties of titania nanotubes functionalized with (3–glycidoxypropyl) trimethoxysilane. *Mater. Chem. Phys.* **2017**, *193*, 290–297.

20. Pawlik, A.; Jarosz, M.; Syrek, K.; Sulka, G.D. Co-delivery of ibuprofen and gentamicin from nanoporous anodic titanium dioxide layers. *Colloids Surf. B Biointerfaces* **2017**, *152*, 95–102.

21. Zhao, L.; Huo, K.; Mei, S.; Wang, W.; Zhang, Y.; Wu, Z. Influence of Annealing on Cytocompatibility of Anodized Nanoscale Titania Surfaces. In Proceedings of the 2010 3rd International Nanoelectronics Conference (INEC), Hongkong, China, 3–8 January 2010; pp. 864–865.

22. Schmitt, J.; Maheshwari, A.; Heck, M.; Lux, S.; Vetter, M. Impedance change and capacity fade of lithium nickel manganese cobalt oxide-based batteries during calendar aging. *J. Power Sources* **2017**, *353*, 183–194.

23. Walter, G.W. The application of impedance spectroscopy to study the uptake of sodium chloride solution in painted metals. *Corros. Sci.* **1991**, *32*, 1041–1058.

24. Bitondo, C.; Bossio, A.; Monetta, T.; Curioni, M.; Bellucci, F. The effect of annealing on the corrosion behaviour of 444 stainless steel for drinking water applications. *Corros. Sci.* **2014**, *87*, 6–10.

25. Randles, J.E.B. Kinetics of rapid electrode reactions. *Discuss. Faraday Soc.* **1947**, *1*, 11–19.

26. Yu, W.Q.; Qiu, J.; Xu, L.; Zhang, F.Q. Corrosion behaviors of TiO_2 nanotube layers on titanium in Hank's solution. *Biomed. Mater.* **2009**, *4*, 065012.

27. Say, W.C.; Chen C.C.; Shiu, Y.H. Monitoring the effects of growing titania nanotubes on titanium substrate by electrochemical impedance spectroscopy measurement. *Jpn. J. Appl. Phys.* **2009**, *48*, 035004.

28. Aziz-Kerrzo, M.; Conroy, K.G.; Fenelon, A.M.; Farrell, S.T.; Breslin, C.B. Electrochemical studies on the stability and corrosion resistance of titanium-based implant materials. *Biomaterials* **2001**, *22*, 1531–1539.

29. Al-Mobarak, N.; Al-Swayih, A. Development of titanium surgery implants for improving osseointegration through formation of a titanium nanotube layer. *Int. J. Electrochem. Sci.* **2014**, *9*, 32–45.

30. Liu, C.; Wang, Y.; Wang, M.; Huang, W.; Chu, P.K. Electrochemical stability of TiO_2 nanotubes with different diameters in artificial saliva. *Surf. Coat. Technol.* **2011**, *206*, 63–67.

31. Al-Swayih, A. Electrochemical characterization of titanium oxide nanotubes fabricated by anodizing in three kinds of electrolytes. *Life Sci. J.* **2014**, *11*, 52–59.

32. Mohan, L.; Anandan, C.; Rajendran, N. Electrochemical behavior and effect of heat treatment on morphology, crystalline structure of self-organized TiO_2 nanotube arrays on Ti–6Al–7Nb for biomedical applications. *Mater. Sci. Eng. C* **2015**, *50*, 394–401.

33. Mohan, L.; Anandan, C.; Rajendran, N. Electrochemical behaviour and bioactivity of self-organized TiO_2 nanotube arrays on Ti–6Al–4V in Hanks' solution for biomedical applications. *Electrochim. Acta* **2015**, *155*, 411–420.

34. Fabregat-Santiago, F.; Barea, E.M.; Bisquert, J.; Mor, G.K.; Shankar, K.; Grimes, C.A. High carrier density and capacitance in TiO_2 nanotube arrays induced by electrochemical doping. *J. Am. Chem. Soc.* **2008**, *130*, 11312–11316.

35. *Standard Specification for Titanium and Titanium Alloy Strip, Sheet, and Plate*; ASTM B265-15; ASTM International: West Conshohocken, PA, 2015.

36. Mandracci, P.; Mussano, F.; Rivolo, P.; Carossa, S. Surface treatments and functional coatings for biocompatibility improvement and bacterial adhesion reduction in dental implantology. *Coatings* **2016**, *6*, 7.

37. Monetta, T.; Acquesta, A.; Carangelo, A.; Bellucci, F. TiO$_2$ nanotubes on Ti dental implant. Part 1: Formation and aging in Hank's solution. *Metals* **2017**, *7*, 167.

38. Spinolo, G.; Chiodelli, G.; Magistris, A.; Tamburini, U.A. Data processing for electrochemical measurements with frequency response analyzers I. Error analysis and accuracy tests. *J. Electrochem. Soc.* **1988**, *135*, 1419–1424.